

## Simple model for deep bed filtration

Jysoo Lee and Joel Koplik

*Benjamin Levich Institute and Department of Physics, City College of the City University of New York, New York, New York 10031*

(Received 5 February 1996)

We present a simple model for deep bed filtration, where particles suspended in a fluid are trapped while passing through a porous filter. A steady state of the model is reached when the filter cannot trap additional particles. We find the model has two qualitatively different steady states depending on the fraction of traps, and the steady states can be described by directed percolation. We study, in detail, the evolution of the distribution of trapped particles, as the number of trapped particles increases. To understand the evolution, we formulate a mean field equation for the model, whose numerical solution is consistent with the behavior of the model. We find the trapped particle distribution is insensitive to details of the formulation of the model. [S1063-651X(96)10310-X]

PACS number(s): 47.55.Mh, 05.40+j, 05.60+w, 64.60.Ak

### I. INTRODUCTION

Deep bed filtration is a well-established process used to separate solid particles suspended in a fluid [1–4]. A dilute suspension is injected into a filter made of porous material. Particles, while flowing through the filter, are trapped inside by various mechanisms. The trapped particles can later be recovered by “cleaning” the filter.

The quantities of main interest are the filter efficiency (the fraction of injected particles trapped in the filter) and the pressure drop across the filter in order to maintain a constant fluid flow. As more particles are trapped in the filter, the filter efficiency usually decreases, and the pressure drop usually increases. The theory of deep bed filtration should predict these quantities in terms of parameters of the system. In order to build such a theory, one needs certain knowledge about the dynamics inside a filter, e.g., the spatial distribution of trapped particles. Unfortunately, such information has been very limited [5,6].

Recently, Ghidaglia *et al.* carried out a series of experiments on deep bed filtration [7–9]. Instead of a conventional porous material (e.g., sandstone), they used a random packing of glass spheres as the filter medium. The transparency of glass and the index matched fluid used for the suspension allow direct visual observation inside the whole filter. The movements of particles can be followed in great detail. The setup can be used to gain valuable information inside the filter, such as the interaction of particles with a porous medium, and the distribution of trapped particles. It also becomes a challenge to understand these newly available quantities.

Network models can be used to study the behavior of particles and a fluid in a filter [10–13]. In a network model, the inner structure of the filter is modeled by pores interconnected by narrow channels. A microscopic pressure-flow relation, e.g., Darcy’s law, is assumed across each channel. Such relations and the external boundary conditions provide equations for the flow field, which can be solved numerically. The motion of a particle is determined by both the local flow field and the interaction between particles. The main advantage of a network model is that it is a good approximation to a real system. For example, the flow field and

the movement of a particle can be calculated from microscopic equations with a reasonable geometry. The disadvantage, however, is large computational efforts necessary even for the simulations of a moderate size system.

Instead, we propose a cellular automata model for deep bed filtration. The main advantage of the model is, due to its simplicity, that one can study the detailed behavior of systems of a fairly large size. Only geometric properties can be obtained from the model. Also, the rules for the movement of particles are too simple to capture the detailed interactions of real particles. For example, the actual flow field in a filter constantly changes with the movement of particles. Such changes are mostly ignored in the present model. We thus expect that only those aspects of the behavior of the model which are not sensitive to the details of the rules can be compared with experiments. Such comparisons are necessary to establish the validity and the limitations of the model.

As the number of trapped particles increases, the model reaches a steady state in which no additional particle can be trapped. The steady state can, as we shall see, be described by directed percolation (DP). The qualitative behavior of the steady state is different depending on a parameter  $p$ , the fraction of trapping bonds. If  $p$  is less than threshold  $p_c$ , a newly injected particle simply pass through the filter without being trapped. On the other hand, if  $p > p_c$ , all the paths leading to an exit are blocked. We study in detail the evolution of the distribution of trapped particles for various values of  $p$ . To understand the behavior of the model, we construct a mean field differential equation for the evolution of the distribution. The numerical solutions of the equation are in good agreement with the simulations of the model. We also find that the behavior of the model is not sensitive to various changes of the rules for the dynamics.

The paper is organized as follows. In Sec. II, we define the model, and study the model without blocking. We form a differential equation, and its solution is compared with the simulations of the model. In Sec. III, we study the steady state of the full model with blocking, and compare it with DP. We also study the evolution of the distribution of trapped particles. In Sec. IV, a few modification of the rules are introduced to check the stability of the behavior of the

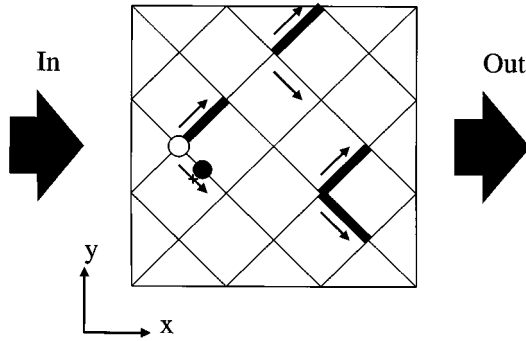


FIG. 1. A schematic view of the model filter: nodes and bonds in the square lattice represent pores and channels in filter, respectively.  $S$  bonds are shown with thin lines, whereas thick lines are used for  $B$  bonds. A moving particle is shown with an empty circle, and a trapped particle with a filled circle. The arrows next to bonds show possible movement of a particle. For example, the particle cannot move to the  $S$  bond with a trapped particle.

model. A brief summary of the results and limitations of the model are given in Sec. V.

## II. MODEL WITHOUT BLOCKING

### A. Definition of the model

Consider a square lattice, rotated by  $45^\circ$  to the flow axis, of width  $W$  and length  $L$ , which is an idealized network model of the filter pore space (Fig. 1). The nodes and bonds of the lattice represent pores and channels, respectively. A periodic boundary condition is applied in the transverse direction. Fluid containing suspended particles is injected on the left side of the filter ( $x=1$  line), and exits the right side ( $x=L$  line). Suspended particles, if not trapped, move along the local direction of the fluid flow. We consider particles of a radius  $R$ , and assign a channel radius  $r_j$  to bond  $j$ , where the radius is drawn from some distribution  $C(r)$ . A bond with  $r_j > R$  is called a  $B$  (big) bond, and other bonds ( $r_j \leq R$ ) are  $S$  (small) bonds. Particles can move through a  $B$  bond without difficulty, while they would be trapped in an  $S$  bond. Let the fraction of  $S$  bonds be  $p$ .

The rules for the movement of a particle are defined as follows. A particle is inserted at a randomly chosen node at the left end. We require that the particle always tries to move to the right, the direction of the fluid flow. At a node, the particle has to choose a bond out of the two bonds on its right for a movement. We first consider the case that no particle is trapped in the bonds. Here, the particle randomly chooses a bond with equal probability. If the chosen bond is a  $B$  bond, the particle moves through the bond to the next node. If it is a  $S$  bond, the particle is trapped in the bond. The movement of the particle is repeated until either the particle is trapped or comes out of the filter. We then insert another particle to the filter, and the whole process is repeated.

We still have to define the rules involving bonds which contain a trapped particle. A reasonable rule is that if a particle is trapped inside a bond, the entrance to the bond is blocked by the particle. Note that only  $S$  bonds can trap a particle. There are two possibilities involving blocked bonds. If only one of the two bonds for the movement is blocked,

we always move the particle to the bond which is not blocked. If both bonds are blocked, the situation becomes a little complicated. The particle can not continue to move, when it reaches such a dead end. We solve the problem by blocking all the paths leading *only* to dead ends. The details of the procedure will be discussed in Sec. III.

The system with the rules defined so far is the main model, which will be studied extensively for the most of the paper. In this section, however, we want to start with a simpler case of no blocking. In this case, a particle can move through an  $S$  bond with a trapped particle, and it will not be trapped. In a sense, an  $S$  bond with a trapped particle is treated like a  $B$  bond. Thus the effect of blocking by a trapped particle is ignored. The model without blocking is not realistic, and its behavior is very different from that with blocking. However, ignoring the effect of blocking makes the analysis of the model tractable, and the method developed here will later be extended to the full model with blocking.

### B. Simulation of the model

We present results of numerical simulations of the model without blocking. The primary quantity of interest is the density field  $\rho(x,t)$  of trapped particles. Here,  $\rho(x,t)dx$  is defined as the number of trapped particles in  $[x, x+dx]$  divided by  $2W$ . Also,  $t$  is the total number of injected particles, which can be used as a timelike variable. In Fig. 2(a), we show  $\rho(x,t)$  for several values of  $t$  and  $p$ . For small  $t$ , the density field forms a characteristic shape—two flat regions joined by a transition region. For large  $t$ , the field seems to translate without much change of shape. If the shape of the field remains constant, one can show that the curve should move with constant velocity  $v(p) = 1/2Wp$ . The velocity is defined as the amount of translation per injected particle. We translate the fields of Fig. 2(a) according to the velocity as shown in Fig. 2(b). The fields for different  $t$  all seem to collapse in a narrow region. A closer inspection shows, however, the shape changes slowly, but systematically, with  $t$ . The width of the transition region slowly increases with  $t$ .

A further point is that the shapes of  $\rho(x,t)$  for different values of  $p$  seem to look the same. One can roughly scale these curves to a single curve as shown in Fig. 2(c). The curves agree very well with each other for small  $t$ . Then, the width of the transition region grows faster for larger values of  $p$ , and systematic deviations from the collapse are visible as  $t$  increases. In scaling the curve, we scale the width of the transition region by  $1/p$ . The argument for the choice follows. For a given  $p$ , the penetration depth of a particle is of order  $1/p$ . The width of the transition region, which is the fluctuation of the penetration depth, is expected to be similar to the penetration depth. In the next section, we show that the simulational results discussed here can be understood in terms of a mean field differential equation for the evolution of  $\rho(x,t)$ .

### C. Evolution equation of the density field

We derive an approximate equation for the evolution of the density field  $\rho(x,t)$ . Consider the motion of a particle injected into the filter. Whenever the particle moves, there is a certain probability that the particle is trapped. The average

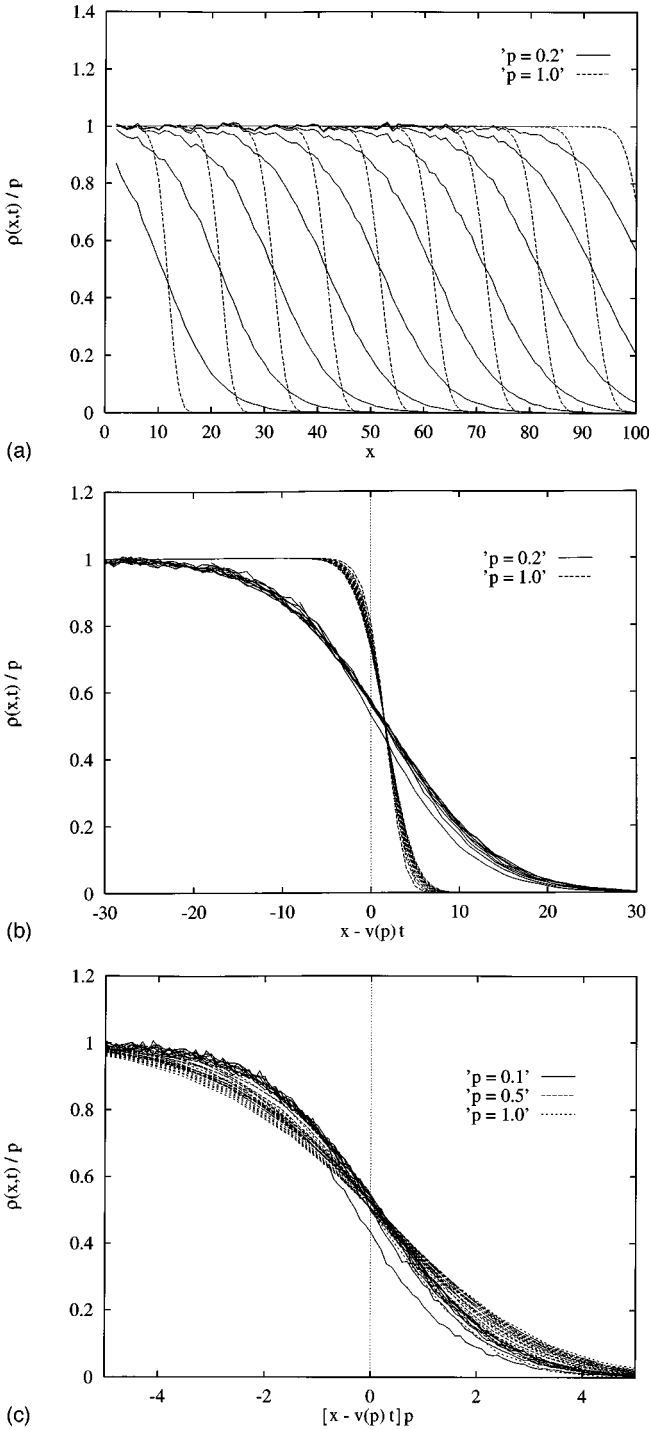


FIG. 2. (a) The density field  $\rho(x,t)$  for  $p=0.2$  and  $1.0$  is shown for several values of  $t$ . The difference of  $t$  between the successive fields is  $10^4 p$ . (b) The fields in (a), translated by  $v(p)t$ , are shown. (c) The scaled fields for  $p=0.1, 0.5$ , and  $1.0$  are shown. The scaled fields collapse very well for small  $t$ , but deviations from the collapse are apparent for large  $t$ . Here, we use  $W=500$  and  $L=100$ , and all the fields are averaged over 100 samples.

fraction of unoccupied  $S$  bonds, which act as traps, at position  $x$  is  $p - \rho(x,t)$ . We assume that the probability that the particle is trapped, while moving from  $x$  to  $x+dx$ , is  $[p - \rho(x,t)]dx$ . Here, an approximation is made which ignores the variation of the density field in the transverse ( $y$ )

direction. Let  $P(x,t)$  be the probability that the particle arrives at position  $x$  without being trapped. Under the above assumption, the probability of the particle to be trapped in  $[x, x+dx]$  is  $[p - \rho(x,t)]P(x,t)dx$ . We thus arrive at

$$\frac{\partial}{\partial x} P(x,t) = -[p - \rho(x,t)]P(x,t), \quad (1)$$

whose solution with condition  $P(0,t) = 1$  is

$$P(x,t) = \exp\left[-\int_0^x p - \rho(x',t) dx'\right]. \quad (2)$$

Since the density field increases by  $1/2W$  for every new particle trapped, the evolution equation for the density is

$$\begin{aligned} \frac{\partial}{\partial t} \rho(x,t) &= \frac{1}{2W} [p - \rho(x,t)] P(x,t) \\ &= \frac{1}{2W} [p - \rho(x,t)] \exp\left[-\int_0^x p - \rho(x',t) dx'\right]. \end{aligned} \quad (3)$$

The derivation of (3) involves another approximation. The change of the density field per injected particle is assumed to be proportional to the trapping probability which is *averaged* over all possible trapping sites (mean field approximation). On the other hand, the relevant density field, and the one we have considered, is obtained by injecting certain number particles (e.g., 10 000) without taking an average after each injection. The average is taken only *after the whole injection* of particles. The two procedures are, in general, not equal. The validity of the approximations in deriving (3) will be checked with simulations of the model.

The evolution equation (3) contains an integral in the exponent, which makes further analysis less convenient. The integral can be eliminated by simple manipulations. Motivated by the wavelike behavior of the density field found in the simulations, we search for a traveling wave solution— $\rho(x,t) = f[x - v(p)t]$ . Inserting it into (3),

$$\begin{aligned} \frac{\partial}{\partial t} f(x-vt) &= -v \frac{\partial}{\partial x} f(x-vt) \\ &= \frac{1}{2W} [p - f(x-vt)] \\ &\quad \times \exp\left[-\int_0^x p - f(x' - vt) dx'\right]. \end{aligned} \quad (4)$$

Differentiating the equation with respect to  $x$ , and after a little rearrangement,

$$\frac{\partial^2}{\partial x^2} f = -\frac{1}{p-f} \left(\frac{\partial}{\partial x} f\right)^2 - (p-f) \frac{\partial}{\partial x} f, \quad (5)$$

which is a nonlinear differential equation.

We cannot obtain the analytic solution of the equation, and we numerically solve it using a Runge-Kutta routine [14]. The solution is calculated in the interval  $[0,10]$ . We choose  $f=p$  at  $x=0$ . The boundary condition at the other

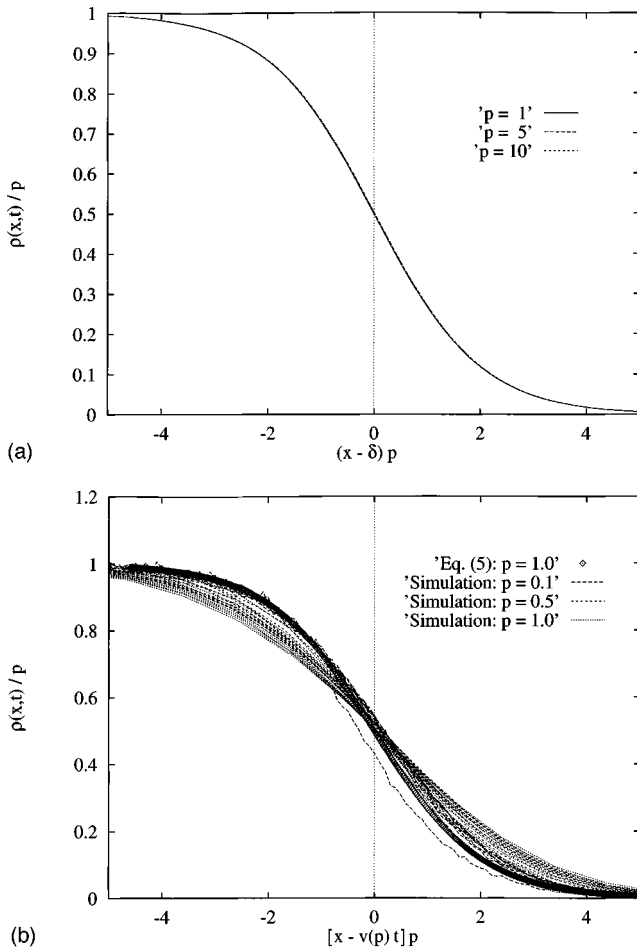


FIG. 3. (a) The solution of (5) for  $p=1,5,10$  is shown. The scaling used for the fields is the one used for the simulational data [Fig. 2(c)]. The fields exhibit excellent scaling behavior. Here, the fields are translated by  $\delta$  so that the centers of the transition regions coincide. (b) The solution for  $p=1$  is shown with the density fields from the simulations. There are good agreements at early  $t$ .

end is a bit subtle. We choose  $f$  to be close to, but not equal to, 0 at  $x=10$ . Note that  $f$  can not be 0 due to the nonzero probability that a particle passes through the interval. We have tried  $f=10^{-3}, 10^{-4}, 10^{-5}$  with no essential difference in the result. The value of  $f$  is chosen to reveal the whole shape of the field in the interval. The value of  $f$  at  $x=10$  changes the amount by which the curve is translated, not the shape of the curve. In Fig. 3(a), we show the numerical solutions of the equation for several values of  $p$ . The shape of the field is very similar to that in Fig. 2. Furthermore, the solutions satisfy the same scaling as the simulations. Here, the scaling is almost perfect without any visible deviation. We also show both the numerical solution and the density fields obtained by the simulations in Fig. 3(b). There is good agreement, especially at early  $t$  of the simulation. However, the width of the transition region of the field from the simulations gradually increases, as  $t$  increases. Equation (3) seems to provide a good overall description of the results of the simulations, except the broadening of the interfaces.

What is the possible origin of the broadening? Think of the filter bed as a set of  $W$  columns perturbed by the transverse coupling between them. The average number of par-

ticles injected in a column is  $n=t/W$ . The fluctuation of  $n$  should be order of  $\sqrt{n}$ . Consider a column in the filter. Since the average position of the transition region in the column is  $\bar{x}=n/2p$ , the fluctuation of  $\bar{x}$  is  $\delta x=\sqrt{\bar{x}/2p}$ . Therefore, the width of the transition region of the *whole* filter is affected not only by the width  $\omega_s$  of the transition region of a single column, but also by  $\delta x$ . A rough estimate is that the resulting width  $\omega$  becomes  $\sqrt{\omega_s^2+(\delta x)^2}$ , which implies that the ratio  $\omega/\omega_s$  is  $\sqrt{1+2p\bar{x}}$ . Thus the effective width increases with  $t(\bar{x})$ , and the rate of the increase is larger for larger  $p$ , which are consistent with the results of the simulations (Fig. 2).

### III. FULL MODEL WITH BLOCKING

#### A. Steady state behavior

Having obtained reasonable understanding of the model without blocking, we proceed to a more interesting case where blocking is present. We first discuss the steady state of the model. It will later become clear that the information of the steady state plays a crucial role in describing the evolution of  $\rho(x,t)$ . A steady state is reached when there are no more empty  $S$  bonds which can be reached by an injected particle, thus the density field  $\rho(x,t)$  will remain constant. Let the steady state density field be  $\rho_s(x)$ . We consider the steady state in the limit of the infinite system size. In the steady state, if  $p < p_c$ , all injected particles pass through the filter without being trapped. On the other hand, if  $p > p_c$ , all the paths leading to an exit from the filter are blocked. Here,  $p_c$  is a threshold. We start to see the similarity of the present model to directed bond percolation (DP) [15]. By comparing the rules of the present model with those of DP on a square lattice, one can notice that the positions of trapped particles in the steady state are identical to those of the blocked bonds connected to a cluster in a DP. We thus expect the steady state density field  $\rho_s(x)$  to be described by DP.

We briefly review predictions of DP. First, there is a percolation threshold  $p_c$ . The exact value of  $p_c$  is not known, and the best estimate for bond percolation on a square lattice is  $0.355\,299(1)$  [16]. Note that  $p$  represents the blocking probability, not the conducting probability commonly used for percolation. We discuss the behavior in three separate regimes.

$p=p_c$ : There exists a spanning cluster of unblocked bonds. The mass of a spanning cluster can be calculated as follows. The probability that a bond belongs to a spanning cluster  $P_\infty(p)$  scales as  $|p-p_c|^\beta$ . Since the correlation length in the longitudinal direction  $\xi_\parallel$  scales as  $|p-p_c|^{-\nu_\parallel}$ ,

$$P_\infty(p) \sim \xi_\parallel^{-\beta/\nu_\parallel}. \quad (6)$$

The total mass of a spanning cluster is  $P_\infty(p)$  times the width  $2W$  and the length  $\xi_\parallel$  of the cluster  $2W\xi_\parallel^{1-\beta/\nu_\parallel}$ . Then, the mass of a spanning cluster in  $[x, x+dx]$  divided by  $2W$ , which behaves the same as  $\rho_s(x)dx$ , is

$$\rho_s(x)dx \sim x^{-\beta/\nu_\parallel}dx. \quad (7)$$

Using the best estimates for  $\nu_\parallel$  and  $\beta$  [1.7334(10) and

0.277(1), respectively],  $\beta/\nu_{\parallel}$  is determined to be 0.1598 [16]. The steady state density field at the threshold  $p_c$  decays as a power law.

$p < p_c$ : There also exists a spanning cluster. Following the formalism in DP, we propose a scaling ansatz

$$\rho_s(x) \sim |p - p_c|^{\beta} g(x/\xi_{\parallel}), \quad (8)$$

where  $g(z)$  is a scaling function to be determined. The scaling is, as in DP, expected to be valid near  $p_c$ . The function  $g(z)$  has to satisfy certain properties. Consider the limit of  $p \rightarrow p_c^-$ , which results in  $\xi_{\parallel} \gg x$ . Since the density field has to approach (7),  $g(z)$  should behave as  $z^{-\beta/\nu_{\parallel}}$  for  $z \ll 1$ . On the other hand, the density field has to approach  $P_{\infty}$  as  $z \gg 1$ , which implies  $g(z) \sim 1$ . In sum,

$$g(z) \sim \begin{cases} z^{-\beta/\nu_{\parallel}} & \text{if } z \ll 1, \\ 1 & \text{if } z \gg 1. \end{cases} \quad (9)$$

$p > p_c$ : There is no spanning cluster. In the regime, we propose a scaling ansatz

$$\rho_s(x) \sim x^{-\beta/\nu_{\parallel}} h(x/\xi_{\parallel}), \quad (10)$$

where  $h(z)$  is another scaling function. If we take the limit of  $p \rightarrow p_c^+$  the density field has to approach (7), which requires  $h(z) \sim 1$  as  $z \ll 1$ . No new information about  $g(z)$  can be obtained in the other limit of  $z \gg 1$ .

We present results of the numerical simulations to compare with the above predictions. In order to obtain a steady state, one can inject particles one by one, until no particle can be trapped, literally following the definition. The procedure is quite time consuming, and there is a much faster way to determine the steady state density field. The method is based on the ‘‘burning’’ algorithm originally used to study the properties of a percolation cluster [17]. The state state density field is determined in a single ‘‘sweep’’ of the system. The method will be discussed in Appendix A. In the insets of Fig. 4(a) and 4(b), we show  $\rho_s(x)$  for several values of  $p$ , determined by the method. The density field at  $p_c$  decays as a power law with an exponent consistent with (7). We then scale these  $\rho_s(x)$  according to the predictions of DP—(8) and (10). All the curves seem to collapse well into two curves, one for  $p < p_c$  [Fig. 4(a)] and the other for  $p > p_c$  [Fig. 4(b)]. Only small deviations can be seen for the values of  $p$  away from  $p_c$ . Note that all the parameters used for the scaling (e.g.,  $p_c, \beta$ ) are those of DP, and no free parameters are used. The scaled curves, which are the scaling functions  $g(z)$  and  $h(z)$ , also satisfy the properties discussed before. The scaled curve of Fig. 4(a), which is  $g(z)$ , decays as a power law for small  $z$ , and approaches a constant for large  $z$ . Also, the curve  $h(z)$  in Fig. 4(b) approaches a constant for small  $z$ , and seems to decay as an exponential. Thus the comparison with the numerical simulations confirms that the steady state density field is well described by DP.

## B. Evolution of the density field

Now we will discuss the evolution of the density field for the full model with blocking. The simulation of the model poses a subtle problem. Consider a particle moving in the

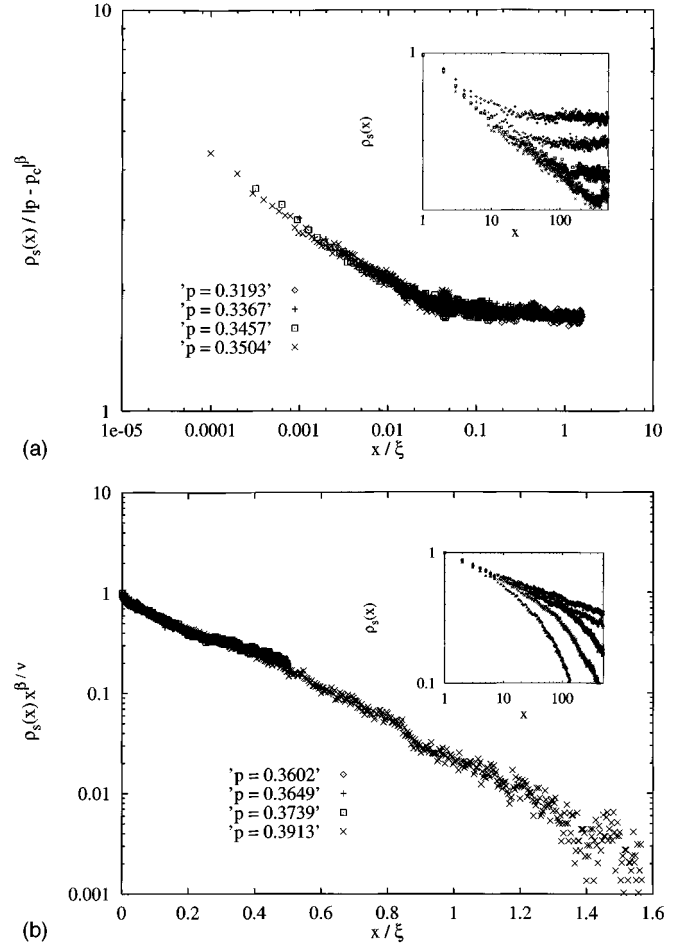


FIG. 4. The scaled steady state density fields  $\rho_s(x)$  of the model with blocking is shown for (a)  $p < p_c$ :  $p = 0.3193, 0.3367, 0.3457, 0.3504$ , and for (b)  $p > p_c$ :  $p = 0.3602, 0.3649, 0.3739, 0.3913$ . The fields before scaling are shown in the insets. Also, the field for  $p = p_c$  is shown in the inset of (b). Here,  $W = 100$ ,  $L = 500$ , and the density fields are averaged over 100 samples.

filter. If both of the bonds available to the particle are blocked, the particle can not continue to move. What should be an appropriate rule for the movement? In a real situation, a particle chooses a channel according to the amount of fluid flow in the channel. Since the fluid flow in the channels leading *only* to dead ends will be very small, particles rarely go to these channels. In the present simulation, we remove all the paths leading *only* to blocked bonds. To identify such a path, one has to consider more than local geometry, since all the paths connected to the bond have to be traced. We have developed a method based on the burning algorithm [17]. The method is similar to the one used to remove the ‘‘dangling’’ bonds of an infinite percolation cluster. The detailed description of the method will be given in Appendix B. In Fig. 5, we show the evolution of the density field for several values of  $p$ . For small  $p$ , the overall shape of the field is similar to the no blocking case (Fig. 2). There are two small differences, though. The steady state value of the density field for  $x \gg 1$  is smaller than  $p$ , compared to the value of  $p$  for the model without blocking. The difference is due to the fact that some of  $S$  bonds are not accessible to injected particles. Also, the width of the transition region for the

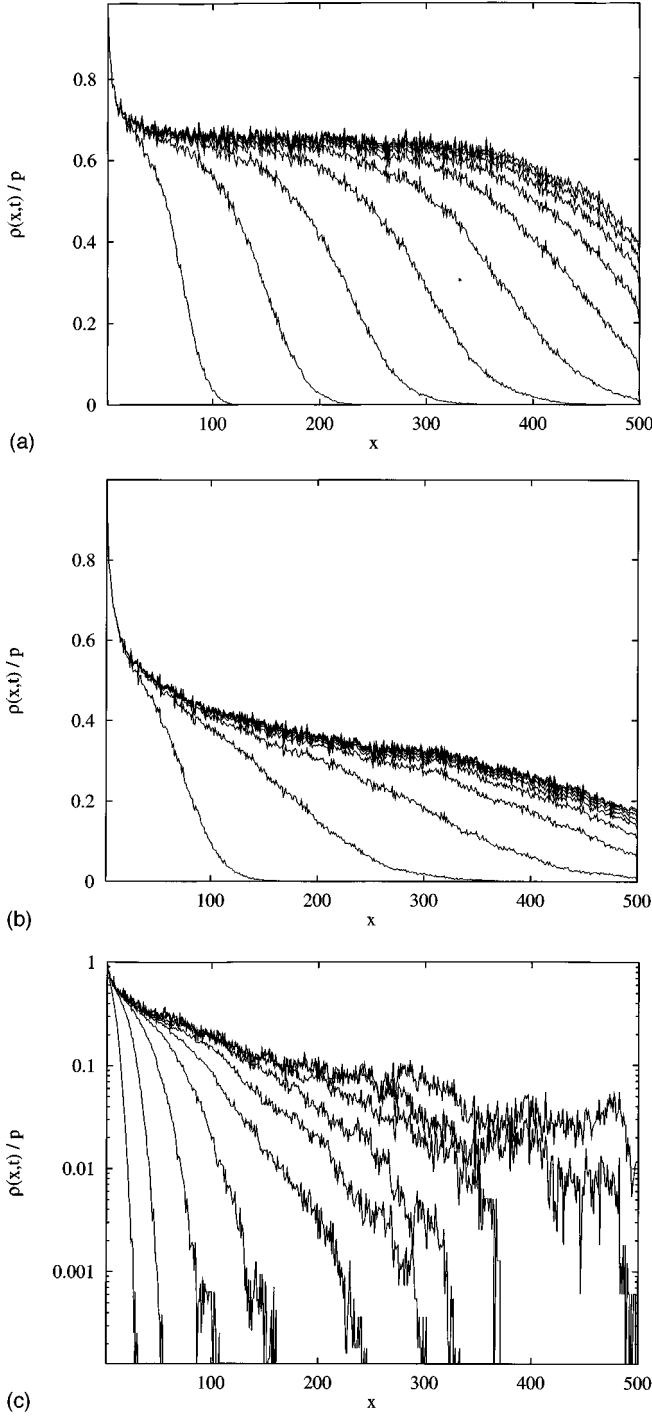


FIG. 5. Evolution of the density field with blocking is shown for (a)  $p=0.3193$ , (b)  $p=p_c$ , and (c)  $p=0.3913$ . Here,  $W=100$ ,  $L=500$ , and the fields are averaged over 100 samples. The difference of  $t$  between the successive fields is 3000 for (a) and (b), and 1000 for (c).

model with blocking is a bit larger. As  $p$  increases, even the overall shape of the field becomes different from that without blocking. The width of the transition region becomes quite large (comparable to the length of the system in some cases). The density field for very small  $t$  is exponential, in agreement with the previous simulations [8].

We quantify the transition region by defining the average position  $\bar{x}$  and the width  $\delta x$  of the region. For  $p < p_c$ , the

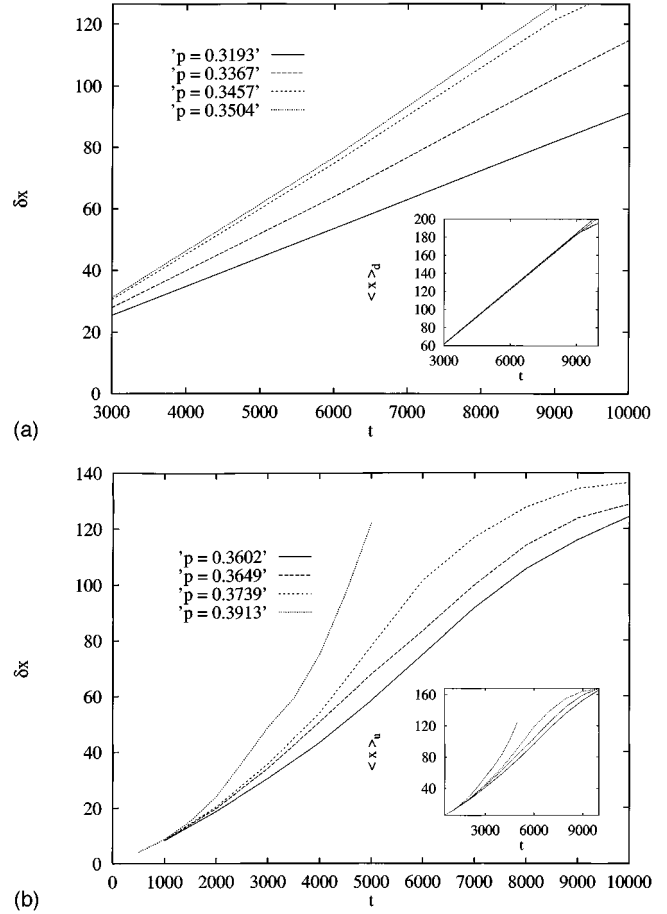


FIG. 6. The mean position and the width of the transition region from the simulation data as in Fig. 5: The width is shown (a) for  $p < p_c$ :  $p=0.3193$ ,  $0.3367$ ,  $0.3457$ ,  $0.3504$ , and (b) for  $p > p_c$ :  $p=0.3602$ ,  $0.3649$ ,  $0.3739$ ,  $0.3913$ . The mean positions are also shown in the insets.

inflection point of the field  $\rho(x,t)$  is a suitable criterion for  $\bar{x}$ . We numerically calculate the spatial derivative  $\rho'(x,t) \equiv -\partial_x \rho(x,t)$  using the smoothed data of  $\rho(x,t)$ . The results are not sensitive to the exact procedure for the smoothing. The resulting field  $\rho'(x,t)$  is a bell shaped curve, where the position of the maximum is the inflection point. We define  $\bar{x}$  and  $\delta x$  as the mean  $\langle x \rangle_d$  and the standard deviation  $\sqrt{\langle x^2 \rangle_d - \langle x \rangle_d^2}$  of  $\rho'(x,t)$ , respectively. Thus  $\langle A \rangle_d$  is defined as

$$\langle A \rangle_d = \frac{\int_0^L \rho'(x,t) A(x,t) dx}{\int_0^L \rho'(x,t) dx}. \quad (11)$$

The average position  $\bar{x}$  and the width  $\delta x$  for several values of  $p$ , where  $p < p_c$ , are shown in Fig. 6(a). Comparing the values with the density fields (Fig. 5) confirms that these values are reasonable representations of the transition region.

Unfortunately, the above procedure cannot be applied for  $p > p_c$ . Here, the inflection point of the field, if it exists, is not a reasonable representation of the mean position of the transition region. The density field behaves like a decaying exponential. We define  $\bar{x}$  and  $\delta x$  as the mean  $\langle x \rangle_u$  and the standard deviation  $\sqrt{\langle x^2 \rangle_u - \langle x \rangle_u^2}$  of  $\rho(x,t)$ , respectively. Thus  $\langle A \rangle_u$  is defined as

$$\langle A \rangle_u = \frac{\int_0^L \rho(x,t) A(x,t) dx}{\int_0^L \rho(x,t) dx}. \quad (12)$$

In Fig. 6(b), the values of  $\bar{x}$  and  $\delta x$  obtained following the procedure are shown. Again, the values seem to be reasonable representations of the transition region.

How do we understand the evolution of the field? Is there any equation similar to (3) which can be used for the situation? To answer the question, we inspect (3) again. In the equation, the trapping probability of a particle passing through a channel is assumed to be  $p - \rho(x,t)$ , the fraction of empty  $S$  bonds. In other words, we assume that *all*  $S$  bonds will eventually trap one particle. One of the effects of blocking is, however, to make some of the  $S$  bonds inaccessible to the injected particle. For the model with blocking, the fraction of accessible  $S$  bonds is  $\rho_s(x)$  instead of  $p$ . It thus seems reasonable to replace  $p$  with  $\rho_s(x)$  in (3), when blocking is allowed. The proposed equation for the model with blocking is

$$\frac{d}{dt} \rho(x,t) = \frac{1}{2W} [\rho_s(x) - \rho(x,t)] \times \exp \left[ - \int_0^x \rho_s(x') - \rho(x',t) dx' \right]. \quad (13)$$

We numerically solve the equation, where we use the steady state density field  $\rho_s(x)$  measured in the preceding section. For quantitative comparisons, we calculate the mean and the width of the transition region of the resulting field using the methods discussed before. In Fig. 7, we show these quantities for several values of  $p$ . By comparing them with the ones obtained by the simulations (Fig. 6), one can notice the overall behavior is essentially identical. Also, even their numerical values are in good agreements. We thus believe that the modified equation (13) is a good starting point for the description of the model with blocking.

#### IV. STABILITY OF THE MODEL

In this section, we study a few variations of the model. Our objectives are twofold: we want the rules to be more realistic, and we want to know how much the results (e.g., the density field) change under the variations. Only the quantities which are not sensitive to the details of the model are meaningful, and can be compared with experiments.

The first variation is to introduce the concept of flow induced probability (FIP) [18,20,19]. Consider a particle moving through filter. As the particle reaches a pore, it has to choose a channel to continue its movement. The exact rule for the choice is complicated, and is not fully understood. Still, it is a good approximation to assume the particle chooses a channel proportional to the amount of flow going through it, which is called flow induced probability. In the present model, the particle chooses a channel with equal probability, if it is not blocked. The problem in introducing FIP to the model is that the flow field for the whole system has to be calculated. The calculation, not only is time consuming, but also goes against our intention of constructing a simple model.

A simple solution for the problem can be obtained by

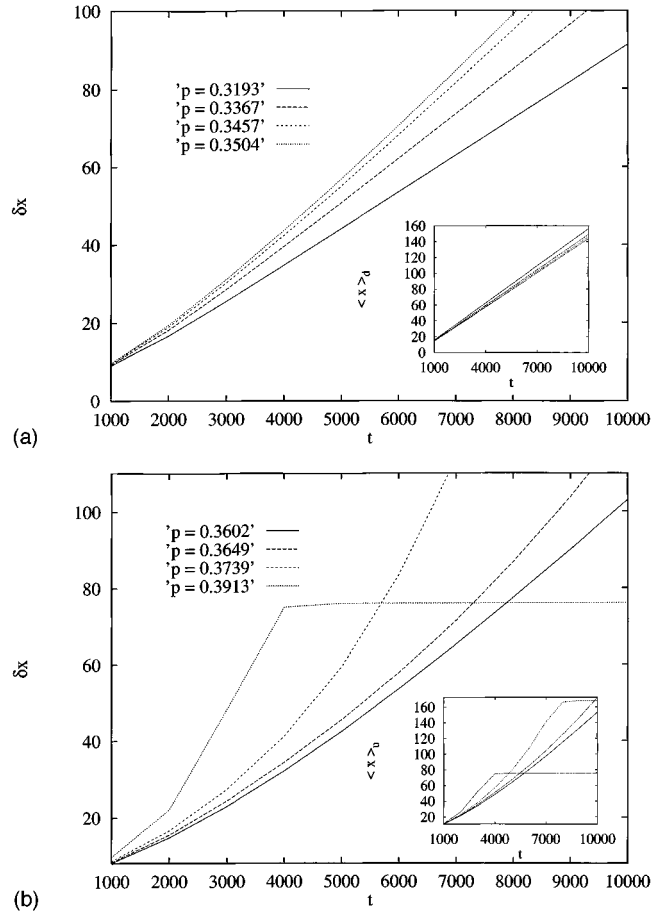


FIG. 7. The mean position and the width of the transition region of the density field obtained from (13): the width is shown (a) for  $p < p_c$ :  $p = 0.3193, 0.3367, 0.3457, 0.3504$ , and (b) for  $p > p_c$ :  $p = 0.3602, 0.3649, 0.3739, 0.3913$ . The mean positions are also shown in the insets.

noting the strong correlation between the flow and the mobility of a channel. It also seems reasonable to assume that they are proportional to each other. Thus we implement FIP by assigning a mobility to channels, and assume the amount of flow in a channel is proportional to its mobility. The mobility of a channel is determined as follows. For a channel, one chooses a radius  $r$  drawn from distribution  $C(r)$ . If one assumes for simplicity that the channel length is on the order of the channel radius, the mobility of the channel is proportional to  $r^3$ , where we assume Poiseuille flow in a cylindrical tube. How about distribution  $C(r)$  for the radius? We first try a uniform distribution in the interval  $[1/2, 1]$ . Thus the probability that the radius is in  $[r, r+dr]$  is  $2dr$ , if  $1/2 < r < 1$ , and is zero for other values of  $r$ . The new rule significantly changes local movements. The probability of choosing a channel can now differ by a factor of 5 to 6. In Fig. 8, we show the density field obtained by the numerical simulations of the uniform distribution for several values of  $p$ . There are small differences between the fields with and without FIP, especially at small values of  $t$ . The resulting difference is quite small, considering the significant changes of particle movements.

We also study the field using  $C(r)$  of the three dimensional random close packing (RCP) of uniform spheres.

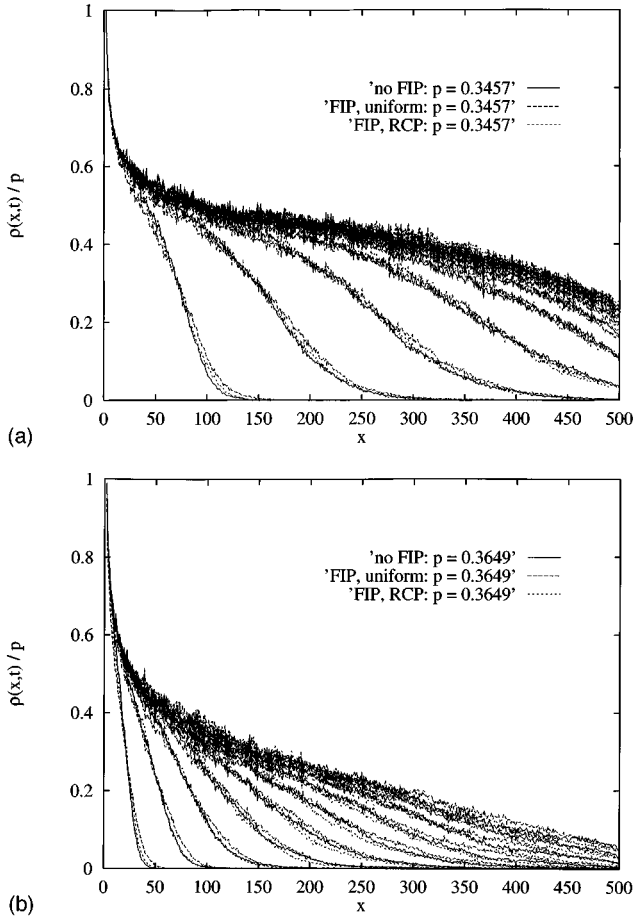


FIG. 8. The evolution of the density field with and without FIP for (a)  $p=0.3457$  and (b)  $p=0.3649$ . Here,  $W=100$  and  $L=500$ , and the averages are taken over 100 samples. The difference of  $t$  between successive density fields is (a) 3000 and (b) 1000, respectively.

Here, we use the data for the radial distribution of RCP in Ref. [21]. The exact procedure to calculate  $C(r)$  from the data is discussed in Appendix C. In Fig. 8, the resulting density field using the distribution of RCP is shown. The field is again a little different from that without FIP, just like the uniform distribution. Flow induced probability does not significantly change the density field. For later comparisons, we also calculate the mean and the width of the transition region, as shown in Fig. 9.

The above implementation of flow induced probability can be included in the framework of the evolution equation. The effect of FIP is that it modifies the effective trapping probability of  $S$  bonds. For a given distribution  $C(r)$ , the probability that a particle to be trapped  $\Pi$  while passing through a channel is

$$\Pi = \frac{\int_0^R \sigma(r) C(r) dr}{\int_0^\infty \sigma(r) C(r) dr}, \quad (14)$$

where  $\sigma(r)$  is the mobility of a channel with radius  $r$ . If uniform conductance  $\sigma(r) = \sigma_0$  is assumed,  $\Pi$  returns to the familiar value of  $p$ , the fraction of  $S$  bonds. The effective distribution of  $C(r)$  changes as particles are trapped in  $S$  bonds, making them inaccessible to further incoming par-

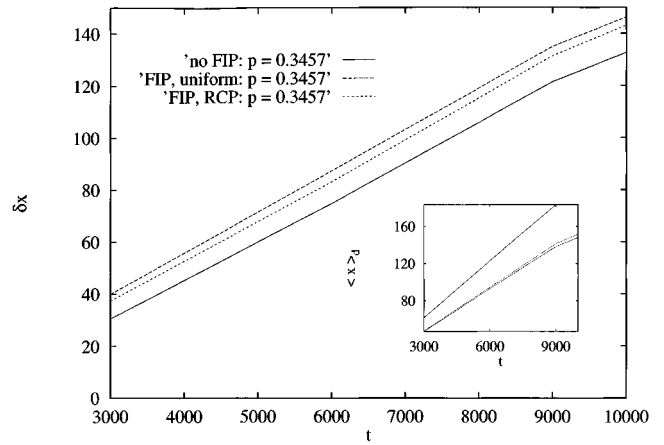


FIG. 9. The mean position (inset) and the width of the transition region for the density fields of Fig. 8(a).

ticles. We model this change by removing blocked  $S$  bonds out of the distribution, and transferring them to  $r > R$  part of the distribution. To be more precise, the effective distribution at given  $t$ ,  $C(r, t)$ , has to satisfy the following conditions:

$$\int_0^R C(r, t) dr = p - \rho(x, t), \quad (15)$$

and

$$\int_R^\infty C(r, t) dr = 1 - p + \rho(x, t). \quad (16)$$

We choose to remove blocked bonds from the  $r < R$  part of the distribution, thus  $C(r, t) = [1 - \rho(x, t)/p]C(r)$ . We then transfer the removed bonds to the  $r > R$  part of the distribution, thus  $C(r, t) = [1 + \rho(x, t)/(1 - p)]C(r)$ . In other words,

$$C(r, t) = \begin{cases} [1 - \rho(x, t)/p]C(r) & \text{if } r \leq R, \\ [1 + \rho(x, t)/(1 - p)]C(r) & \text{if } r > R. \end{cases} \quad (17)$$

Thus the probability to trap a particle passing through a channel located at  $x$  at time  $t$  is

$$\Pi(x, t) = \frac{[1 - \rho(x, t)/p]P_L}{[1 - \rho(x, t)/p]P_L + [1 + \rho(x, t)/(1 - p)]P_R}, \quad (18)$$

where  $P_L = \int_0^R \sigma(r) C(r)$  and  $P_R = \int_R^\infty \sigma(r) C(r)$ . The effect of blocking can be added by replacing  $p$  with  $\rho_s(x)$  in the above equation. The resulting equation for the evolution is

$$\frac{d}{dt} \rho(x, t) = \frac{1}{2W} \Pi(x, t) \exp \left[ - \int_0^x \Pi(x', t) dx' \right]. \quad (19)$$

We numerically solve the equation with blocking. In order to compare the simulations with FIP, we calculate the mean and the width of the transition region as shown in Fig. 10. Comparing the solution with the numerical simulations (Fig. 9), one notice good agreements between them, which gives more confidence in the evolution equation.

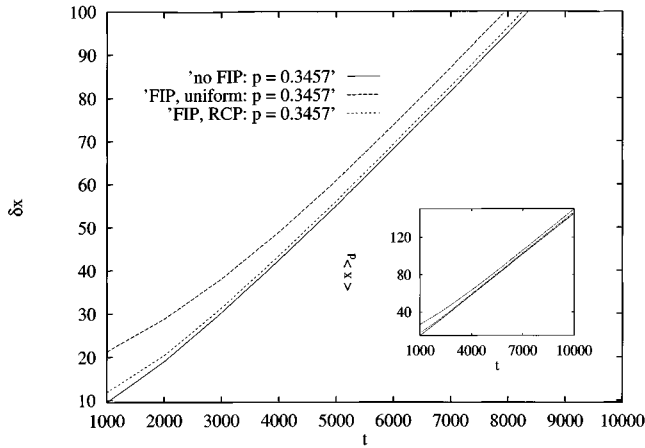


FIG. 10. The mean position (inset) and the width of the transition region from the numerical solution of the evolution equation (19) are shown.

Finally, we study the effect of the relaunching observed in experiment [8]. There, when a particle passes near a trapped particle, it occasionally kicks the trapped particle out of its site. The kicked (or “relaunched”) particle can be trapped again, or it can move along the fluid flow. The actual mechanism for the relaunching, which is probably due to hydrodynamic interaction, is not completely understood. Here, we use a simple rule, which tries to imitate the effect. Consider a particle at a node. If one of the channels right of the node has a trapped particle, the trapped particle will be kicked out of the bond with probability  $q$ . Once the particle is relaunched, it moves just like any other particle [8]. In Fig. 11, we show the density field obtained for several values of  $p$  and relaunching probability  $q$ . In the simulations, flow induced probability is included, and the distribution  $C(r)$  of RCP is used. One can see the relaunching changes the density field a little. The density field does not seem to be sensitive to the details of the rules.

## V. CONCLUSION

In this paper, we have studied a simple model for deep bed filtration. The primary quantity of interest is the density field of trapped particles. The evolution of the density field is significantly different depending on whether  $p$  is below or above a threshold  $p_c$ . The density field and its evolution do not seem to depend on the details of the rules. In order to have some theoretical understanding of the model, we have proposed a mean field equation for the evolution. The equation seems to describe well both qualitative and quantitative behaviors of the model.

There are several things one should examine before taking the present model seriously. First of all, one has to check how sensitively the results depend on the details of the rules. The rules we have used for particle movements—choosing a channel, the effect of blocking and the relaunching of trapped particle—are too simple to be realistic. Thus only behavior which is not sensitive to the rules can be compared with experiments. Here, we have studied a few variations of the rules, and have found the behavior is not sensitive to the changes, but more extensive study in this direction is desir-

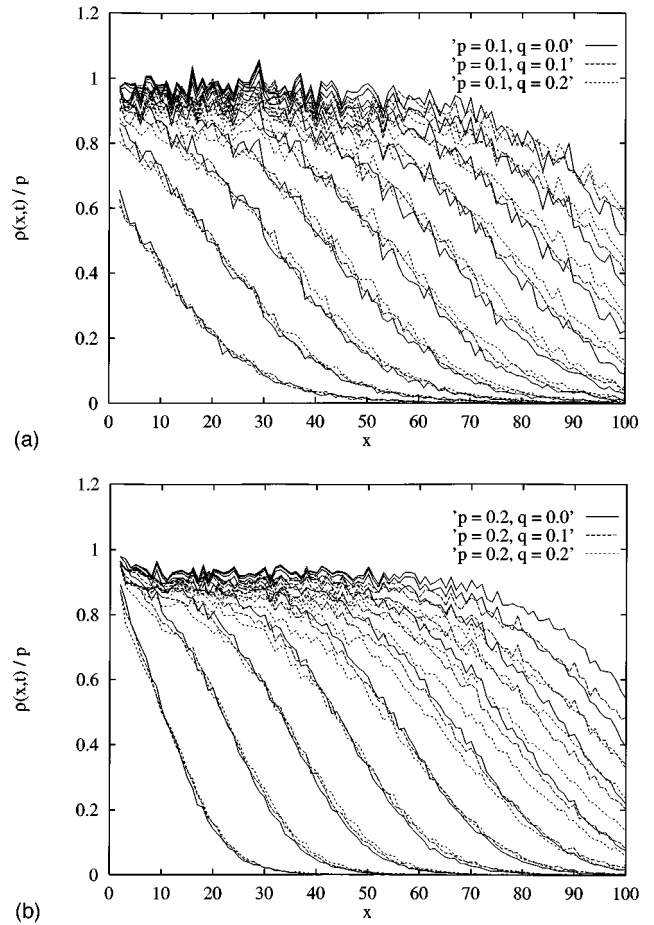


FIG. 11. The evolution of the density field with relaunching is shown for several values of  $q$  and for (a)  $p=0.1$  and (b)  $p=0.2$ . Here,  $W=100$ ,  $L=100$ , and the field is averaged over 100 samples. Here, we use  $C(r)$  of RCP, and flow induced probability is included.

able. The crucial next step to check the relevance of the model to experiments, however, is to compare with network models [22]. Network models are believed to be a faithful representation of real porous media. For example, the changes in the flow field due to particle movements are taken into account in these models. If the simple model compares well with network models, it can be used as a complimentary tool to study deep bed filtration, and, in particular, the large scale behaviors of the system.

## ACKNOWLEDGMENTS

We thank E. Guazzelli, C. Ghidaglia, L. de Arcangelis, and S. Redner for extensive discussions. We also thank E. J. Hinch for helpful discussions and drawing our attention to Ref. [14]. This work is supported by the Department of Energy under Grant No. DE-FG02-93-ER14327.

## APPENDIX A: DETERMINATION OF THE STEADY STATE

We describe the algorithm we use to find all accessible  $S$  bonds. Consider the square lattice shown in Fig. 1. We assign variable  $c(x,y)$  to node  $(x,y)$ , and set its value to

0. We start by setting  $c(x,y)=1$  at all the nodes on  $x=1$  line. We then check the nodes on  $x=1$  line. For site  $(1,j)$ , we check the two bonds connected right to the node. If the bond is an  $S$  bond, we mark it as  $T$ . If the bond is  $B$  bond, we set  $c(x,y)=1$  at the node connected to  $(1,j)$  node through the bond. Having checked the nodes on  $x=1$  line, we proceed to check the nodes along  $x=2$  line. If  $c(2,j)=1$ , we update the bonds and the nodes connected to the  $(2,j)$  node as described before. We repeat the procedure until  $x=L$  line. After the update, the bonds marked as  $T$  are the bonds which trap a particle in the steady state.

#### APPENDIX B: REMOVING THE DEAD ENDS

We describe the algorithm we use to remove all the paths which lead *only* to dead ends. The essential idea is to start from a dead end, and trace back all the paths leading to it. To be precise, consider a network as shown in Fig. 1. We start from the right end of the filter,  $x=L-1$  line. We check all the nodes at the line. For node  $(L-1,y)$ , we check if both of the bonds to the right the node are blocked. If both of them are blocked, we block the entrance to the node. In other words, we block any  $B$  bond left to the node. We do not have to worry about  $S$  bonds, since incoming particles will block them. After checking all the dead ends at  $x=L-1$  line, we go to  $x=L-2$  line. We check if both of the bonds to the right of the node  $(L-2,y)$  are blocked, and block appropri-

ate  $B$  bonds if necessary. We repeat the procedure until  $x=1$  line. After the sweep, all the paths leading only to dead ends are blocked.

#### APPENDIX C: CALCULATION OF $C(r)$ OF RCP

We describe the method we use to calculate the channel radius distribution  $C(r)$  for the three dimensional random close packing (RCP) of monosize spheres. In essence, we can calculate  $C(r)$  from the nearest neighbor distribution  $N(r)$  of RCP, where  $N(r)dr$  is the number of neighbors whose center lies  $[r,r+dr]$  away from the center of a reference particle. We use the data for  $N(r)$  in Ref. [21]. We scan the figure of  $N(r)$  to obtain a postscript bitmap image file. Then, we read the coordinates of nonempty pixels from the file. After simple rescaling,  $N(r)$  can be reconstructed from the pixel coordinates. From  $N(r)$ , we generate three lengths  $r_{12}$ ,  $r_{23}$ , and  $r_{31}$ . Here,  $r_{ij}$  is the center-to-center distance between sphere  $i$  and  $j$ . We take the channel size as the radius of the sphere which barely fits in the hole formed by the three spheres. The present method ignores the correlation between the neighbor distances (e.g.,  $r_{12}$  and  $r_{23}$ ). However, the comparisons of polygons and polyhedrons generated by the present method with those by actual measurements confirm that the method is an excellent approximation [21]. The channel radius distribution obtained here agrees well with the one in Ref. [21].

- 
- [1] J. Herzig, D. Leclerc, and P. LeGoff, *Ind. Eng. Chem.* **62**, 8 (1970).
- [2] S. Goren, in *Physical Separations*, edited by M. Freeman and J. FitzPatrick (Engineering Foundation, New York, 1977).
- [3] J. Dodds, G. Baluais, and D. Leclerc, in *Disorder and Mixing*, edited by E. Guyon, J. Nadal, and Y. Pomeau (Kluwer, Dordrecht, 1988).
- [4] C. Tien, *Granular Filtration of Aerosols and Hydrosols* (Butterworths, Boston, 1989).
- [5] O. Lamrous, D. Houi, C. Zarcone, and J. Pradere, *Rev. Phys. Appl.* **24**, 607 (1989).
- [6] D. Houi, in *Hydrodynamics of Dispersed Media*, edited by J. Hulin, A. Cazabat, and E. Carmona (Elsevier, Dordrecht, 1990).
- [7] C. Ghidaglia, E. Guazzelli, and L. Oger, *J. Phys. D* **24**, 2111 (1991).
- [8] C. Ghidaglia, L. de Arcangelis, J. Hinch, and E. Guazzelli, *Phys. Fluid A* **8**, 6 (1996).
- [9] C. Ghidaglia, L. de Arcangelis, J. Hinch, and E. Guazzelli, *Phys. Rev. E* **53**, 3028 (1996).
- [10] M. Leitzement, P. Maj, J. Dodds, and J. Greffe, in *Solid Liquid Separation*, edited by J. Gregory (Ellis, Harwood, 1984).
- [11] S. Rege and H. Fogler, *AIChE J.* **34**, 1761 (1988).
- [12] M. Sahimi and A. Imdakm, *Phys. Rev. Lett.* **66**, 1169 (1991).
- [13] J. Hampton, S. Savage, and R. Drew, *Chem. Eng. Sci.* **48**, 1601 (1993).
- [14] After the paper was written, it was pointed out to us that the analytic solution of the equation was obtained by E. J. Hinch and B. S. Bhatt, *J. Fluid Mech.* **212**, 279 (1990).
- [15] D. Stauffer, *Introduction to Percolation Theory* (Taylor & Francis, London, 1985).
- [16] J. Essam, A. Guttmann, and K. Da'Bell, *J. Phys. A* **21**, 3815 (1988).
- [17] H. Herrmann, D. Hong, and H. E. Stanley, *J. Phys. A* **17**, L261 (1984).
- [18] P. G. Saffran, *J. Fluid Mech.* **6**, 321 (1959).
- [19] S. Rege and H. Fogler, *Chem. Eng. Sci.* **42**, 1553 (1987).
- [20] M. Sahimi, H. Davis, and L. Serwer, *Chem. Commun.* **23**, 329 (1983).
- [21] G. Mason, *Nature* **217**, 735 (1968).
- [22] J. Lee and J. Koplik (unpublished).